# Fast Track

**Zi Rui Li**[1]
**Gui Rong Liu**[1, 2]
**Yu Zong Chen**[1, 3]
**Jian-Sheng Wang**[1, 4]
**Hansen Bow**[5]
**Yuan Cheng**[2]
**Jongyoon Han**[5, 6*]

[1]The Singapore-MIT Alliance, Singapore
[2]Centre for ACES, Department of Mechanical Engineering, National University of Singapore, Singapore
[3]Department of Pharmacy, National University of Singapore, Singapore
[4]Department of Physics, National University of Singapore, Singapore
[5]Department of Electrical Engineering and Computer Science, Massachusetts Institute of Technology, Cambridge, MA, USA
[6]Department of Biological Engineering, Massachusetts Institute of Technology, Cambridge, MA, USA

Received September 11, 2007
Revised November 6, 2007
Accepted November 26, 2007

## Continuum transport model of Ogston sieving in patterned nanofilter arrays for separation of rod-like biomolecules

This article proposes a simple computational transport model of rod-like short dsDNA molecules through a microfabricated nanofilter array. Using a nanochannel consisting of alternate deep wells and shallow slits, it is demonstrated that the complex partitioning of rod-like DNA molecules of different sizes over the nanofilter array can be well described by continuum transport theory with the orientational entropy and anisotropic transport parameters properly quantified. In this model, orientational entropy of the rod-like DNA is calculated from the equilibrium distribution of rigid cylindrical rod near the solid wall. The flux caused by entropic differences is derived from the interaction between the DNA rods and the solid channel wall during rotational diffusion. In addition to its role as an entropic barrier, the confinement of the DNA in the shallow channels also induces large changes in the effective electrophoretic mobility for longer molecules in the presence of EOF. In addition to the partitioning/selectivity of DNA molecules by the nanofilter, this model can also be used to estimate the dispersion of separated peaks. It allows for fast optimization of nanofilter separation devices, without the need of stochastic modeling techniques that are usually required.

**Keywords:**
DNA electrophoresis / Electroosmotic flow / Filtration / Nanofluidics / Ogston sieving
DOI 10.1002/elps.200700679

## 1 Introduction

The electrophoretic migration of polyelectrolyte in polymeric gels forms the foundation of gel separation of biomolecules such as DNA, RNA, and proteins [1]. According to the Ogston–Morris–Rodbard–Chrambach (OMRC) model [2–4], the gel electrophoretic mobility of biomolecules is determined by the characteristic size of the random porous network and that of molecules in solution. It is found that OMRC model is applicable to the cases of small molecule electrophoresis with low electrical fields and low gel concentrations. For more complicated cases, more sophisticated models and extensive calculations are required [5]. Although a large number of modifications have been suggested for OMRC model trying to address the problem of hindered transport of biomolecules with arbitrary shapes through porous gels, the interpretation of experimental data for even simple, rod-like cylindrical molecules is still far from satisfactory [6]. It has been realized that, in addition to the characteristic sizes of the molecule and the gel pore, comprehensive interpretation of experimental data for systems involving anisotropic solutes requires information about entropic barrier that

**Correspondence:** Zi Rui Li, The Singapore-MIT Alliance, Singapore, Singapore
**E-mail:** smalzr@nus.edu.sg
**Fax:** +65-67791459

**Abbreviations: OMRC model,** Ogston–Morris–Rodbard–Chrambach model; **SPH,** smoothed particle hydrodynamics

* Additional corresponding author: Dr. Jongyoon Han, E-mail: jyhan@mit.edu

originates from reduction of the orientational freedom of polyelectrolytes in small pores of polymeric gels [7]. The coupled effects of anisotropy of solutes and irregularity in geometry of random pores of the polymeric gel make the analysis of fractionation outcome complicated. To achieve better understanding of the sieving process involved in gel electrophoresis, quantitative characterization on a well-characterized model system is desirable. Patterned periodic regular sieving structures are found to be ideal for the study of molecular dynamics and electromigration of polyelectrolytes because the dimension of obstacles and channels can be precisely measured and controlled [8, 9]. Han and his group have used an array of microfabricated filtration device with regions of two different depths to study the migration of long DNA [10, 11], rod-like short DNA [12, 13], and small proteins [14]. For typical nanofilter array (used for Ogston sieving of small biomolecules) as shown in Fig. 1, the depths of the wells are in the scale of 1 μm while those of the slits are less than 100 nm. As the effective sizes of the migrating molecules (rod length of the short DNA) are in the same order or larger than the depth of the slits (nanofilter gap size), the entry into the restricted nanofilter slits requires the DNA molecules to be positioned and oriented properly without interfering with the nanofilter wall. This steric constraint forms an orientational entropy barrier for the transport of DNA and plays a major role in the electrophoretic separation of DNAs over such repeated nanofilter arrays. Theoretical size selectivity of such nanochannels has been addressed empirically based on experimental observations and the basic equilibrium models [12]. However, optimization of the nanofilter separation system would require an efficient computational model that can estimate the performance of different device structures in terms of both separation selectivity (partitioning) and dispersion. Simulations of the same system, based on dissipative particle dynamics [15, 16] and Brownian dynamics [17], have recently been reported. However, these types of stochastic modeling techniques tend to be computationally expensive. Also, these simulations often track only a single molecule in the nanochannel system, and therefore are not well suited for modeling the peak dispersion behavior, which is another important figure of merit of the nanofilter separation systems.

In this article we report a simulation study of the electrophoretic separation of rod-like dsDNA molecules in the patterned nanofilter arrays based on continuum transport theory. Unlike previous simulations, this continuum theory provides a platform to fully describe sieving, diffusion, and convection of a band of biomolecules passing through a repeated array of nanofilters. In this theory, the degree of freedom in a DNA's orientations is projected into an orientational entropy term, using statistical theory for the equilibrium distribution of rigid cylindrical molecules near solid channel walls. Stochastic interaction of the DNA rod with the wall has been averaged and captured into a single entropy-driven transport term in the master flux equation. In addition, the effects of the spatial confinement of nanochannel to the DNA's mobility and translational diffusion coefficient are quantified using statistical theory for the equilibrium distribution. Numerical analysis is performed using a model nanofilter array consisting of 20 repeats of unit cells. From the translation and broadening of peaks over these repeats, the results of separation of the DNA molecules passing through the full-length channel (consisting of $10^4$ repeats) are calculated. It will be shown that the entropic barrier effect, combined with the modified anisotropic transport parameters in the confined nanofilter space, accounts for the fractionation of the DNA molecules of different sizes.

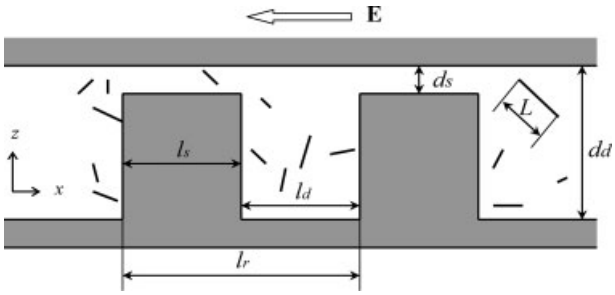


**Figure 1.** The nanofilter for separation of rod-like rigid DNA molecules. Each unit cell consists of a deep well and a shallow slit. The repeat length $l_r$ is the sum of length of the shallow slit $l_s$ and that of the well $l_d$. The slit depth $d_s$ is normally comparable to the length of the migrating molecules $L$, while the depth of deep well, $d_d$ is larger than $L$. The configurational restriction in the shallow slits forms an entropy barrier that varies with the length of molecules. In addition, anisotropic distribution of configurations results in changes in diffusion coefficient and electrophoretic mobility when a DNA is located in a confined space of the nanochannel. As a result, DNA molecules of different lengths are trapped for different time durations when an external electric field **E** is applied to drive the migration of these DNA molecules.

## 2 Methods

### 2.1 Transport theory of the rod-like DNA

The electrophoretic transport of rod-like DNA molecules over nanofilter array is formulated as the migration of charged Brownian particles in a viscous fluid driven by a static external electric field. The concentration of DNA molecules is assumed to be dilute enough so that the intermolecular interactions between DNA molecules can be ignored. It is also assumed that the external electric field is not affected by the presence of DNA molecules and other ions.

As shown in Fig. 2a, a DNA rod has both translational and orientational degrees of freedom. If we assume that the rotational Brownian motion of a DNA molecule is much faster than electric field driven translation, so that there exists a state of local orientational equilibrium for a DNA rod with its center located at any point in the nanochannel, the orientational degrees of freedom of the DNA rod can be eliminated by averaging of the orientation-dependent quan-

 

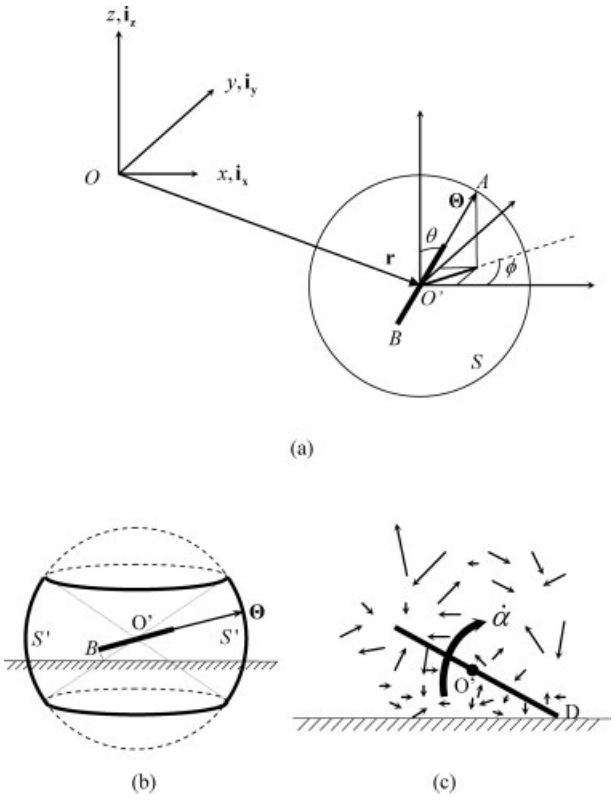


**Figure 2.** (a) The position and orientation of a DNA rod. Axes *Oxyz* represent a global system. Vector **r** denotes the position of center of the DNA. Vector $\boldsymbol{\Theta} = (\theta,\phi)$ represents the unit vector ($|O'A| = 1$) locked into the DNA rod ($|O'B| = L/2$) and lies along the rod's long axis. The surface of the unit sphere is represented by *S*, corresponding to all the possible orientations of the rod. (b) Permissible and forbidden orientations of the DNA rod near a solid wall. The surface represented by *S'* corresponds to permissible orientations while the others ($S - S'$) shown by dashed curves are forbidden. (c) When one end of a DNA rod (*D*) hits the wall at rotational velocity ($\dot{\alpha}$, shown by the thick arrow) during rotational Brownian motion, that end stops instantaneously as its motion is hindered in all directions while other portions of the rod retain their original rotational velocities owing to the sustained random thermal fluctuations of the surrounding fluid molecules (shown by the irregular thin arrows).

tities with their Boltzmann probabilities. The validity of this assumption is guaranteed by the high rotational diffusion coefficients of short rod-like DNAs. At room temperature, the rotational diffusion coefficients ($D^r$) for 50, 150, and 300 base pairs (bp) DNA molecules are in the order of $10^4 \sim 10^6$ rad$^2$/s. In a typical traveling time (0.05 – 0.1 s) through one 1.0 μm repeat under electric field strengths in our experiments, angular variances $\sigma_\alpha^2 = 4D^r t$ are estimated as $10^3 \sim 10^6$ rad$^2$. As the recognizable rotation angle lies in the range $0 \sim \pi/2$, a DNA molecule is able to sample all accessible orientations many times. Hence a state of local rotational equilibrium exits. In addition, the effect of nonuniform electric field lines on the angular distribution of the DNA molecule under the electric field strengths we studied is found negligible compared with that of rotational Brownian motion. Therefore, the orientational distribution of a DNA rod is approximately uniform in free solution. Consequently, electric field driven migration of DNA rods can be modeled as the transport of point-sized charged particles in the aqueous solutions.

Let $C \equiv C(\mathbf{r},t)$ denote the concentration of DNA molecules at a point $\mathbf{r} = (x, y, z)$ at time $t$, a unified electrochemical potential $\mu \equiv \mu(\mathbf{r},t)$ can be defined as [18]

$$\mu = \mu^0 + RT \ln C + q\Phi - TS \tag{1}$$

Here $\mu^0$, $R$, $T$, $q$, and $\Phi \equiv \Phi(\mathbf{r})$ denote the reference standard-state potential, the gas constant, the absolute temperature, the effective charge of the DNA, and the external electric filed potential, respectively. Scalar field function $S \equiv S(\mathbf{r})$ is the orientational entropy of the rigid DNA rod which captures the stochastic distribution of its orientations in the presence of solid channel walls. The spatial gradient of this unified potential $\nabla\mu$ constitutes a driving force that generates a flux of the DNA in the solvent. According to Eq. (1), $\nabla\mu$ consists of forces from three independent factors, namely thermal diffusion, electric force, and entropic gradient, respectively. Consequently, the fluxes induced from these forces are the sum of their respective contributions, that is

$$\mathbf{J} = -(\mathbf{D}^d \nabla C + \mathbf{U}^e C \nabla\Phi - U^S C T \nabla S) \tag{2}$$

where $\mathbf{D}^d \equiv \mathbf{D}^d(\mathbf{r})$ and $\mathbf{U}^e \equiv \mathbf{U}^e(\mathbf{r})$ are the tensors of diffusion coefficient (in unit of cm$^2$/s) and electrophoretic mobility (in $\mathrm{m \cdot s^{-1} \cdot V^{-1}}$), respectively. The scalar $U^S$, which we refer to as *entropic mobility* in this article, represents the mobility associated with the gradient of orientational entropy (an *entropic force*). This mobility captures the stochastic interactions of a DNA with the solid wall. It has a unit of $\mathrm{m \cdot s^{-1} \cdot mol^{-1} \cdot N^{-1}}$ and equals to the velocity of the DNA obtained if 1 N of force is applied to 1 mol of DNA molecules. The evolution of the concentration of DNA is governed by the mass conservation law

$$\frac{\partial C}{\partial t} = -\nabla \cdot \mathbf{J} \tag{3}$$

This article simulates the electrophoretic transport of the rod-like DNAs by solution of master Eqs. (2) and (3) with no-flux boundary conditions.

### 2.2 Translational diffusion coefficient and the electrophoretic mobility of a DNA near a solid wall

A DNA rod has two different translational hydrodynamic friction coefficients, denoted by $\zeta_\parallel^d$ and $\zeta_\perp^d$, respectively, for the motion parallel and perpendicular to its long axis under thermal fluctuation, gravity, and other nonelectrostatic forces [19–21]. As a result, the translational diffusion coefficient is orientation dependent. When a DNA is oriented at $\boldsymbol{\Theta} = (\theta,\phi)$ as shown in Fig. 2a, its translational diffusion coefficient is given by tensors [19]

 

$$\mathbf{D}^{\mathrm{d}}(\boldsymbol{\Theta}) = D_{\parallel}^{\mathrm{d}}\boldsymbol{\Theta}\boldsymbol{\Theta} + D_{\perp}^{\mathrm{d}}(\mathbf{I}-\boldsymbol{\Theta}\boldsymbol{\Theta}) \tag{4}$$

where $D_{\parallel}^{\mathrm{d}} = k_{\mathrm{B}}T/\zeta_{\parallel}^{\mathrm{d}}$ and $D_{\perp}^{\mathrm{d}} = k_{\mathrm{B}}T/\zeta_{\perp}^{\mathrm{d}}$ are the coefficients of the rod for translational diffusion parallel and perpendicular to the rod's axis, respectively; $\mathbf{I} = \mathbf{i_x i_x} + \mathbf{i_y i_y} + \mathbf{i_z i_z}$ denotes the physical space identity tensor; $k_{\mathrm{B}}$ is the Boltzmann constant.

Similarly, the orientation-dependent electrophoretic mobility is given by

$$\mathbf{U}^{\mathrm{e}}(\boldsymbol{\Theta}) = U_{\parallel}^{\mathrm{e}}\boldsymbol{\Theta}\boldsymbol{\Theta} + U_{\perp}^{\mathrm{e}}(\mathbf{I}-\boldsymbol{\Theta}\boldsymbol{\Theta}) \tag{5}$$

where $U_{\parallel}^{\mathrm{e}} = q/\zeta_{\parallel}^{\mathrm{e}}$ and $U_{\perp}^{\mathrm{e}} = q/\zeta_{\perp}^{\mathrm{e}}$ are the coefficients of the rod for electric-driven motion parallel and perpendicular to the rod's axis, respectively. Here translational hydrodynamic friction coefficients for electric-driven motion, $\zeta_{\parallel}^{\mathrm{e}}$ and $\zeta_{\perp}^{\mathrm{e}}$, are not necessarily equal to their corresponding values for diffusion, $\zeta_{\parallel}^{\mathrm{d}}$ and $\zeta_{\perp}^{\mathrm{d}}$, respectively. The reason is that these two are different physical phenomena [22, 23]. When a DNA is diffusing or moving due to nonelectrostatic forces, its surrounding counterions will move with it, while in the electric field, the counterions will be driven by the electric field to move in the opposite direction.

At the rotational equilibrium state, the mean translational diffusion coefficient and the mean electrophoretic mobility at position **r** are given by

$$\mathbf{D}^{\mathrm{d}}(\mathbf{r}) = \int\int_{\mathrm{S}} p(\boldsymbol{\Theta}|\mathbf{r})\mathbf{D}^{\mathrm{d}}(\boldsymbol{\Theta})\mathrm{d}^2\boldsymbol{\Theta} \tag{6}$$

and

$$\mathbf{U}^{\mathrm{d}}(\mathbf{r}) = \int\int_{\mathrm{S}} p(\boldsymbol{\Theta}|\mathbf{r})\mathbf{U}^{\mathrm{d}}(\boldsymbol{\Theta})\mathrm{d}^2\boldsymbol{\Theta} \tag{7}$$

respectively, where $p(\boldsymbol{\Theta}|\mathbf{r})$ denotes the probability that the rod is orientated at $\boldsymbol{\Theta}$ when its center is located at point **r**; $\mathrm{d}^2\boldsymbol{\Theta} = \sin\theta\mathrm{d}\theta\mathrm{d}\phi$ is the areal element on the surface of the unit sphere $S = \{0 \le \theta < \pi;\ 0 \le \phi < 2\pi\}$. These position-specific $\mathbf{D}^{\mathbf{d}}(\mathbf{r})$and $\mathbf{U}^{\mathbf{e}}(\mathbf{r})$ serve as the respective transport parameters in the expressions of flux given by Eq. (2).

When the DNA lies in the bulk solution, or when it is located such that there is no intersection between the rod and the wall at any orientation, all its orientations are accessible at an equal probability of $p(\boldsymbol{\Theta}|\mathbf{r}) = (4\pi)^{-1}$. In this circumstance, the mean diffusion coefficient and the mean electrophoretic mobility are isotropic [19]. The tensors $\bar{\mathbf{D}}^{\mathrm{d}}$ and $\bar{\mathbf{U}}^{\mathrm{e}}$ are given by $\bar{\mathbf{D}}^{\mathrm{d}} = \mathbf{I}\bar{D}^{\mathrm{d}}$ and $\bar{\mathbf{U}}^{\mathrm{e}} = \mathbf{I}\bar{U}^{\mathrm{e}}$, where, the scalars

$$\bar{D}^{\mathrm{d}} = \frac{(D_{\parallel}^{\mathrm{d}} + 2D_{\perp}^{\mathrm{d}})}{3} \tag{8}$$

and

$$\bar{U}^{\mathrm{e}} = \frac{(U_{\parallel}^{\mathrm{e}} + 2U_{\perp}^{\mathrm{e}})}{3} \tag{9}$$

correspond to the diffusion coefficient and the free-solution electrophoretic mobility that are obtained experimentally [1, 23–30]. Equations (8) and (9) enable us to estimate the values of $D_{\parallel}^{\mathrm{d}}$, $D_{\perp}^{\mathrm{d}}$, $U_{\parallel}^{\mathrm{e}}$, and $U_{\perp}^{\mathrm{e}}$ from $\bar{D}^{\mathrm{d}}$ and $\bar{U}^{\mathrm{e}}$ directly using the established relationships $D_{\parallel}^{\mathrm{d}} \approx 2D_{\perp}^{\mathrm{d}}$ [21, 31] and $U_{\parallel}^{\mathrm{e}} \approx 2U_{\perp}^{\mathrm{e}}$ [25, 32]. To determine $D_{\parallel}^{\mathrm{d}}$, $D_{\perp}^{\mathrm{d}}$, $U_{\parallel}^{\mathrm{e}}$, and $U_{\perp}^{\mathrm{e}}$ using the excremental data relieves us from the complicated task of determining the hydrodynamic coefficients and effective charges for the DNA molecules [23, 24, 33, 34].

It should be noted that while the relationship of $D_{\parallel}^{\mathrm{d}} \approx 2D_{\perp}^{\mathrm{d}}$ is well established [21, 31], the relationship between the $U_{\parallel}^{\mathrm{e}}$ and $U_{\perp}^{\mathrm{e}}$ is not so simple. It has been shown that $U_{\perp}^{\mathrm{e}}$ is dependent on $\kappa_{\mathrm{D}}a$ ($\kappa_{\mathrm{D}}$ is the Debye–Hückel parameter and $a$ is the radius of the DNA) in contrast to$U_{\parallel}^{\mathrm{e}}$, which is $\kappa_{\mathrm{D}}a$-independent [32]. In the low $\kappa_{\mathrm{D}}a$ regime, the Debye length $\kappa_{\mathrm{D}}{}^{-1}$ is comparable or larger than the width of the DNA ($a$), so that hydrodynamic drag to the surrounding fluid occurs just as in the nonelectrophoresis case. In this circumstance, the dynamics of the rod is dominated by the simple hydrodynamic interactions, *i.e.*, $U_{\parallel}^{\mathrm{e}} \approx 2U_{\perp}^{\mathrm{e}}$. However, when $\kappa_{\mathrm{D}}a$ becomes large, there will not be any difference $U_{\parallel}^{\mathrm{e}}$ and $U_{\perp}^{\mathrm{e}}$ because the Debye screening effect takes the dominant role. Under our experimental conditions, $\kappa_{\mathrm{D}}a \approx 1$, the relationship $U_{\parallel}^{\mathrm{e}} \approx 2U_{\perp}^{\mathrm{e}}$ holds approximately.

When a DNA rod is located in a confined space as shown in Fig. 2b, some of its orientations are forbidden due to the presence of solid channel walls. The ratio of the number of permissible orientations to the total number of orientations is

$$\rho(\mathbf{r}) = \int\int_{S'} (4\pi)^{-1}\mathrm{d}^2\,\boldsymbol{\Theta} \tag{10}$$

with $S'$ representing the domain corresponding to permissible orientations on the surface of the unit sphere centered at **r**. The probability of the orientation is then given by

$$\rho(\boldsymbol{\Theta}|\mathbf{r}) = \begin{cases} [4\pi\rho(\mathbf{r})]^{-1} & \text{if orientation } \boldsymbol{\Theta} \text{ is permissible at } \mathbf{r} \\ 0 & \text{otherwise} \end{cases} \tag{11}$$

Substituting Eqs. (4), (5), (10), and (11) to Eqs. (6) and (7) and integrating these two equations yield the position specific diffusion coefficient $\mathbf{D}^{\mathbf{d}}(\mathbf{r})$ and the electrophoretic mobility $\mathbf{U}^{\mathrm{e}}(\mathbf{r})$ required by Eq. (2).

### 2.3 Orientational entropy and entropic mobility of the rod-like DNA

According to the statistical mechanics theory, orientational entropy of a rigid molecule is generally defined as $S(\mathbf{r}) = k_{\mathrm{B}}\ln\Omega(\mathbf{r})$, where $\Omega(\mathbf{r})$ is the accessible microscopic orientation state integrals at point **r** [35]. For the rod-like rigid DNA molecules specifically, the orientational entropy of interest can be rather simply expressed by $S(\mathbf{r}) = k_{\mathrm{B}}\ln\kappa(\mathbf{r})$, where $\kappa(\mathbf{r})$ is the local partition function (defined as the ratio of number of accessible microscopic configurations at **r** near

 

the solid wall to those in the bulk liquid) [35]. As this $\kappa(\mathbf{r})$ is exactly the ratio $\rho(\mathbf{r})$ given by Eq. (10), the entropy is given by

$$S(\mathbf{r}) = k_B \ln \rho(\mathbf{r}) \tag{12}$$

Based on this formulation, a DNA molecule acquires maximum entropy of value 0 when it is located in the bulk solution. As the DNA is located close to a solid wall, a portion of its orientational space is not accessible and therefore the orientational entropy decreases to a negative value. A negative entropy causes no problem here as only the gradient of entropy enters the expression of the flux in Eq. (2).

Another important parameter is the mobility associated with the entropic force. By definition, $U^S$ corresponds to the velocity of a rigid DNA obtained if 1 N of "entropic force" is applied to 1 mol of DNA molecules. Although this quantity is not available through experimental observation, we can derive it based on some qualitative assumptions.

The entropic force in this article is originated from the reactive force that the solid wall applies to a rigid rod when this rod hits the solid wall through rotational motion starting from a permissible orientation. As the energy of thermal fluctuation in each dimension is $k_BT/2$ for both rotational and translational diffusions, we derive the expression of $U^S$ through the comparison between the speeds of the motion at the center of a rod caused by these two types of diffusions.

The free-solution diffusion coefficient and the rotational diffusion coefficient of the short rod-like DNA molecules are given by [27]

$$\overline{D}^d = \frac{k_B T}{3\pi\eta_0 L}\left(\ln\left(\frac{L}{d}\right) + \nu\right) \tag{13}$$

and

$$D^r = \frac{3k_B T}{\pi\eta_0 L^3}\left(\ln\left(\frac{L}{d}\right) + \delta\right) \tag{14}$$

respectively, where $\eta_0$ is the viscosity of the solvent, $L$ and $d$ are the length (given by Kratky-Porod model [36, 37]) and diameter of the DNA rod (≈2 nm), respectively. The parameters $\nu$ and $\delta$ represent the correction terms as the end effect for DNA rods. Neglecting the end effect terms $\delta$ and $\nu$ in Eqs. (13) and (14), the relationship between $\bar{D}^d$ and $D^r$ is $D^r = 9\bar{D}^d/L^2$. Within a typical time duration $\tau$, the 1-D average diffusion angle of the DNA rod in bulk solution is $<\alpha> = (2D^r\tau)^{1/2}$, corresponding to an effective angular velocity $<\dot{\alpha}> = (2D^{r/\tau})^{1/2}$ [21].

When one end of a DNA molecule hits the solid wall during rotation, it is assumed that the tip of this end stops instantaneously and the other portions of the rod rotate at the same speed as that before hitting (Fig. 2c). This assumption is based on the nature of the near-wall thermal diffusions of nanoparticles [38]. The amplitudes of the thermal fluctuations of solid particles and the surrounding fluids decrease when they approach the wall. The particles or the portions of an object that are further from the solid wall are subjected to a higher degree of thermal motion, while motions of those on the solid surface are hindered. As shown in Fig. 2c, at the moment when one end of the DNA (end *D*) hits the wall at a rotational velocity, the motion of end *D* is hindered in *xy*-plane by stationary fluid (no-slip boundary condition), $-z$-direction by solid wall. The motion in $+z$-direction is also not possible at this moment because of the momentum of the whole rod. Therefore, we assume *D* is fixed instantaneously. As long as the thermal fluctuations of surrounding fluids are not affected by the event that the DNA hits the wall, the fluids will continue to push the other portions of the rod to rotate at its original velocity $\dot{\alpha}$ and induces a translational motion for the center of the DNA. Consequently the translational velocity at the center of the rod is $<\dot{r}_r> = <\dot{\alpha}>L/2$, which can be further expressed as $<\dot{r}_r> = (9\bar{D}^d/2\tau)^{1/2}$.

From the translational diffusion point of view, during the same time duration of $\tau$, the 1-D average translational diffusion speed is $<\dot{r}_t> = (2\bar{D}^d/\tau)^{1/2}$. Comparing the velocity of the center of the rod caused by hindered rotational diffusion and that induced by translational diffusion, we can find the relationship of $<\dot{r}_r> = 9<\dot{r}_t>/4$. This relationship tells us that the speed caused by the rotational diffusion near the solid wall (entropic force) is 9/4 times that of the translational diffusion. Therefore, we have

$$U^S = 9U^d/4 \tag{15}$$

where $U^d = \bar{D}^d/RT$ is the mobility of DNA rods in translational diffusion.

### 2.4 Effect of the EOF

The finite charge of the solid channel wall leads to the EOF of the solution [39, 40]. As the surface properties of the solid channel and the depth of the Debye layer are difficult to obtain, the electroosmotic mobility is difficult to determine *ab initio*. Fortunately, it is well known that, in the limit of thin Debye layer (under high ionic strength conditions), the profile of EOF is similar to that of the electric field [16, 41]. Thus, the effect of such an EOF can be modeled through modification of electrophoretic mobility of DNA molecules. In this circumstance, the electrophoretic mobility of DNA molecules ($\bar{\mathbf{U}}^e(\mathbf{r})$ in Eq. 2) is to be replaced by an effective electrophoretic mobility $\bar{\mathbf{U}}^e(\mathbf{r}) + \mathbf{I}U_{EEO}|\nabla\Phi(\mathbf{r})|/E_{av}$, where $U_{EEO}$ is the electroosmotic mobility and $E_{av}$ is the external field strength. Based on comparison between the simulation results and experimental results, it was found that the electroosmotic mobility in this study is about 4/5 of the DNA's free-solution electrophoretic mobility.

### 2.5 Numerical method for discretization and integration

The method of smoothed particle hydrodynamics (SPH) discretizes the problem domain and the governing partial

 

differential equations using a set of particles. In such a method, an arbitrary continuous field function $A(\mathbf{r})$ and its derivatives $\partial A(\mathbf{r})/\partial \mathbf{r}$ at position $\mathbf{r}$ are approximated as the weighted summation of their respective values over the nearest neighboring particles $\mathbf{r}_j$, ($j = 1, 2, \ldots, M$) within the supporting domain of through a smoothing function $W(r)$, where $r = ||\mathbf{r}-\mathbf{r}_j||$ and $M$ is the number of particles in the supporting domain. Since its invention in 1977 [42], these methods have been successfully applied in many areas such as astrophysics, fluid flows, material modeling, and other multidisciplinary fields [43–45]. As all the calculations are performed in a local support domain and the time integration is done explicitly, they are very efficient in computation. The SPH method enables us to simulate a multiple repeat nanochannel using structural data of only one repeat. The detailed theoretical aspects of SPH, the definition/requirements of the kernel function $W(r)$, and the integration of the governing partial differential equations can be found in ref. [43].

In our work, a unit cell of nanofilter is discretized with an assembly of 6000 particles, each of which represents a fraction of DNA solution within the nanoarray. All the field functions including DNA concentration, electric field, orientational entropy, flux density, *etc.* are calculated at the centers of these particles. Specifically, the electric potential is calculated through solving the Laplace's equation $\nabla^2\Phi = 0$, with insulating conditions $\partial\Phi/\partial\mathbf{n} = 0$ on the channel walls ($\mathbf{n}$ is the normal vector of surface of the channel wall). Orientational entropy, translational diffusion coefficient, and electrophoretic mobility are calculated from Eqs. (12), (6), and (7), respectively, with $\rho(\mathbf{r})$ and $p(\mathbf{\Theta}|\mathbf{r})$ determined numerically by enumerating all possible values of $\mathbf{\Theta}$ and checking their hindrances at position $\mathbf{r}$. Master transport Eqs. (2) and (3) are discretized and integrated using these smoothed particles to obtain the evolution of DNA concentrations within the model channel over time. Concentration profiles along the channel axis are obtained by the summation of the amount of DNA molecules in all the particles having the same coordinate along the channel axis.

## 3 Results and discussion

In our experiments, the nanofilter is structurally a succession of the 2-D cells, each of which consists of a deep region and a shallow region. The specifications of the nanofilter cell are $d_s = 60$ nm, $d_d = 240$ nm, and $l_s = l_d = 500$ nm. The total length of the nanochannel is $\widetilde{L} = 1$ cm, corresponding to a repeat number of $n = 10\,000$. Solutions of DNA molecules of 50, 150, and 300 bp are injected to the nanofilter channel under the electric field strengths of 57, 29, and 14 V/cm, respectively. Evolution time and band widths are obtained at the end of the channel and are shown in Figs. 3 and 6, respectively. We simulate these processes using the same unit cell geometry, DNA sizes, and electric fields, and the results are compared with the experimental ones.

Instead of modeling the full channel length, our numerical simulation is performed using a model nanochannel consisting of 20 repeats. Periodic boundary conditions are applied to this 20-repeated structure in order to provide appropriate boundary effects. At $t = 0$, the concentration of the DNA molecule is set as 1.0 (arbitrary unit) within a narrow band in the left side of the first repeat and the concentration in other regions is zero. For $t>0$, the time and position

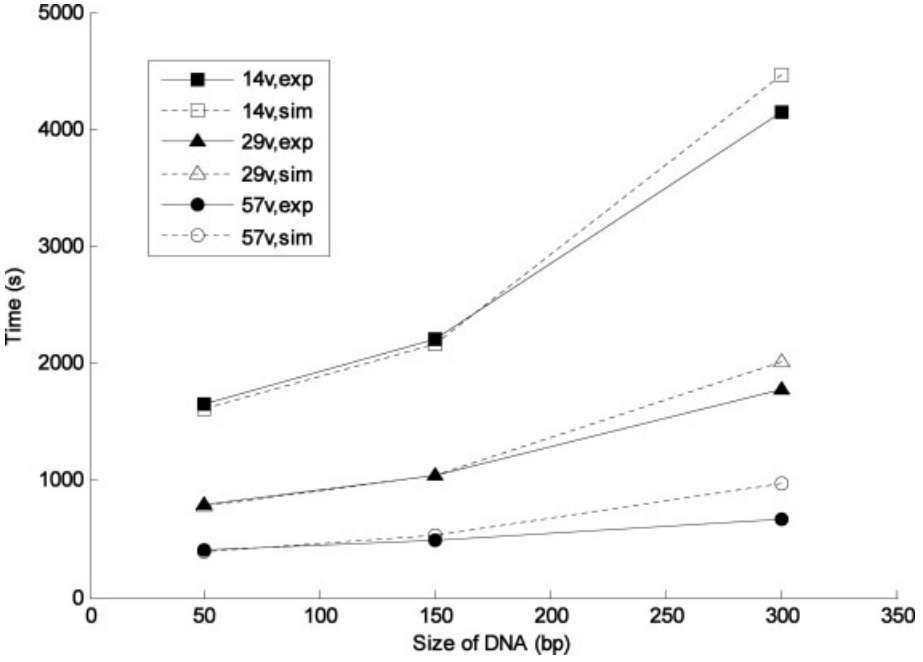


**Figure 3.** Comparison of simulated evolution times with the experimental ones. The simulation evolution times agree well with their corresponding experimental data for 50 and 150 bp DNA molecules. For a 300 bp DNA, its evolution time is overestimated in the simulation due to overestimated entropy barrier.

 

dependent DNA concentrations are obtained through integration of Eq. (3) with no-flux boundary conditions ($\mathbf{J}\cdot\mathbf{n}=0$) at the channel walls. The simulation results show that the concentration profiles along the channel axis are complicated because of the partitioning between the alternate wells and slits. However, when we focus on time-dependant concentration values at the end of each repeat, we find that these values are well described by a Gaussian zone undergoing constant translation and broadening [46].

### 3.1 Effective zone formation and evolution

Assuming that the initial peak width is zero, the shape of the zone undergoing constant spreading and translation observed at time $t$ by a detector located at a distance $\widetilde{L}$ takes the form [46]

$$\gamma(\widetilde{L},t)=\frac{\widetilde{n}}{\sqrt{2\pi}\sigma_{\mathrm{T}}}\exp\left[-\frac{(\widetilde{L}-\widetilde{V}t)^2}{2\sigma_{\mathrm{T}}^2}\right] \tag{16}$$

where $\widetilde{n}$ is the amount of the DNA; $\widetilde{V}$ is the apparent traveling velocity; and $\sigma_{\mathrm{T}}^2$ is the spatial variance of the Gaussian zone. By assumption, $\sigma_{\mathrm{T}}^2$ increase linearly with respect to $t$, that is

$$\sigma_{\mathrm{T}}^2=\Gamma t \tag{17}$$

where $\Gamma$ denotes the combined zone broadening rate as the DNA molecules are passing through the filtration device. The peak passing time at distance $\widetilde{L}$ is obtained from the solution of equation $\partial\gamma/\partial t=0$

$$t^{\mathrm{p}}(\widetilde{L})=\frac{-\Gamma+\sqrt{\Gamma^2+4\widetilde{L}^2\widetilde{V}^2}}{2\widetilde{V}^2} \tag{18}$$

In our simulation, we obtain the peak passing time $t^{\mathrm{p}}(\widetilde{L}_{\mathrm{i}})$ at the end of each repeat $\widetilde{L}_{\mathrm{i}}=i\cdot l_{\mathrm{r}}, i=1,2,\ldots,n$. Parameters $\widetilde{V}$ and $\Gamma$ are estimated from curve fitting using Eq. (18). Once $\Gamma$ and $\widetilde{V}$ are known, evolution time and dispersion of the DNA at the end of channel of any length can then be calculated accordingly.

This expression of peak passing time in Eq. (18) approaches the widely adopted one $t^{\mathrm{p}}(\widetilde{L})=\widetilde{L}/\widetilde{V}$ when $\widetilde{L}\gg\Gamma/\widetilde{V}$. Therefore, as long as the channel length $\widetilde{L}$ is significantly larger than the plate height $H=\Gamma/\widetilde{V}$, or the number of plates are significantly greater than 1, electrophoretic velocity can be estimated from

$$\widetilde{V}=\widetilde{L}/t^{\mathrm{p}}(\widetilde{L}) \tag{19}$$

However, the maximum channel length is 20 μm in our model, while the plate height is about 1–9 μm, corresponding to the number of plates of 2–22. Therefore, we are not able to estimate the parameters $\Gamma$ from the peak width at half height, and $\widetilde{V}$ from Eq. (19), which are widely adopted in experimental studies.

Figure 3 shows the simulation and experimental results of evolution times of DNA molecules of various sizes subjected to different electric fields over 1 cm nanochannel. The simulation results are in good agreement with the experimental ones for 50 and 150 bp DNAs. However, the traveling time for 300 bp DNA is overestimated in this simulation. This difference has to be attributed to the factors that are not considered in our simulation model. As the persistence length of dsDNA is about 50 nm (~150 bp), DNA segments of 300 bp are deformable under thermal fluctuations. In our simulation, however, DNA molecules are treated as rigid rods, thereby the entropy barrier at confined region is overestimated compared with the actual deformable molecules. The result of this overestimation is that the traveling time of the 300 bp DNA is longer than the experimental results.

### 3.2 Effects of spatial confinement on the diffusion coefficient and the effective electrophoretic mobilities in the shallow channels

When a DNA molecule is located in the confined space of a nanochannel, some of its orientations are forbidden due to the presence of the channel wall. For the nanofilter shown in Fig. 1, the probability that DNA molecules are aligned in the $x$-direction is much higher than that in $z$-direction if the dimension of the nanofilter is comparable to the length of the DNA. As a result, components of the electrophoretic mobility and diffusion coefficient in $x$-direction are larger than their counterparts in $z$-direction. The longer the rod is, the higher these differences are. In order to evaluate the effect of this spatial confinement on the transport parameters, we define relative diffusion coefficient and relative electrophoretic mobility as the ratio of their values in confined space to their respective isotropic free-solution values, that is

$$\mathbf{D}'=\frac{<\mathbf{D}^{\mathrm{d}}>}{\bar{D}^{\mathrm{d}}} \tag{20}$$

and

$$\mathbf{U}'=\frac{(<\mathbf{U}^{\mathrm{e}}>+U_{\mathrm{EEO}})}{(\bar{U}^{\mathrm{e}}+U_{\mathrm{EEO}})} \tag{21}$$

respectively, where the bracket $<\cdot>$ represents the average over all the particles in a specific domain. Among all the components in the tensor $\mathbf{D}'$and $\mathbf{U}'$, $D'_{\mathrm{xx}}$, and $U'_{\mathrm{xx}}$ have the most significant effect as the external force are applied in this direction and the motions in other directions are confined or canceled by each other.

Figure 4 shows the values of $D'_{\mathrm{xx}}$ and $U'_{\mathrm{xx}}$ of DNA rods of different sizes in deep and shallow regions of the nanoarray. It could be seen that the effective electrophoretic mobility is increased by ~40% for a 300 bp DNA in the shallow region in $x$-direction compared with free-solution value, while the increase for a 50 bp DNA is less than 10% based on the structure of the nanoarray under investigation.

 

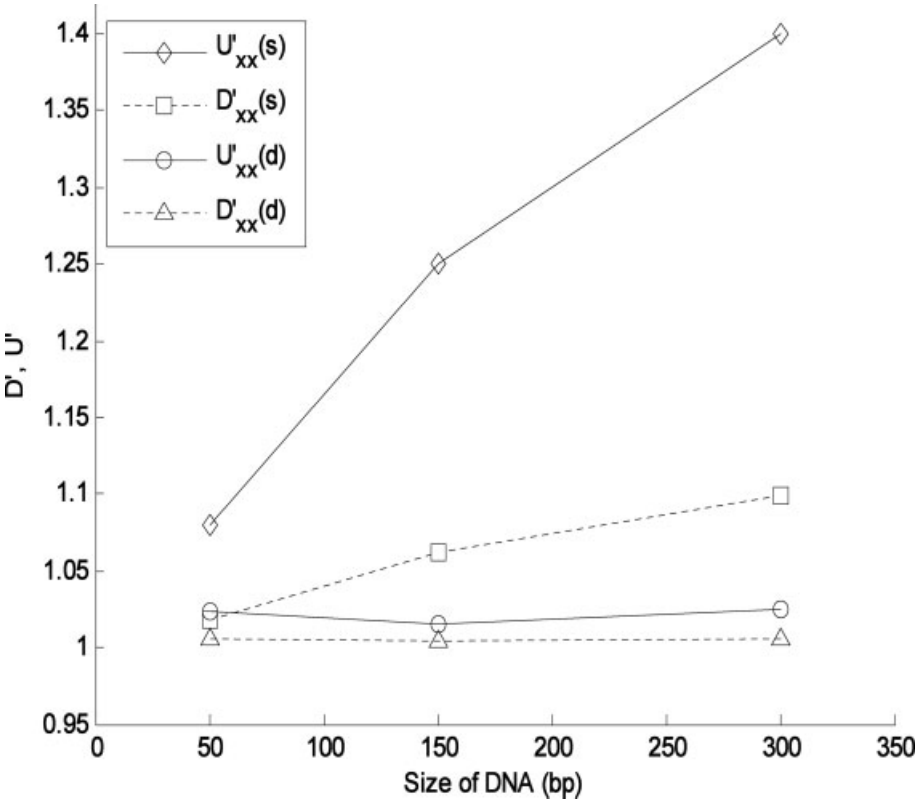


**Figure 4.** Dependence of the relative diffusion coefficients and relative electrophoretic mobilities on the sizes of DNA molecules in deep wells (*d*) and shallow slits (*s*) of the nanofilter. Only components in the direction of channel axis ($D'_{xx}$ and $U'_{xx}$) are shown because the effects of other components are much weaker due to spatial confinement in their relevant directions. The relative diffusion coefficient $D'_{xx}$ is close to 1.0 at all conditions, indicating that the spatial confinement does not affect the diffusion coefficient significantly. In contrast, the relative electrophoretic mobilities are affected by the EOF and may induce very large changes in $U'_{xx}$. In the cases where $U_{EEO} \sim -\bar{U}^e$, a small deviation in $< U^e_{xx} >$ from $\bar{U}^e$ yields a much larger $U'_{xx}$, which will change the final mobility significantly. For the studied experimental conditions here, the effective mobility of 300 bp DNA rod is about 1.4 times of that in bulk solution in the shallow region of the nanofilter ($d_s$ = 60 nm).

Such modification in the electrophoretic mobility may produce a totally different sequence of evolution peaks compared with that from wide channels where $\mathbf{D}^{\mathbf{d}}$ and $\mathbf{U}^{\mathbf{e}}$ are approximately isotropic. The diffusion coefficient is also affected by the constraints in the orientation space, but its magnitude is much smaller than that of the effective electrophoretic mobility.

### 3.3 Normalized mobility and size selectivity

The normalized mobility $U^*$ of the DNA through the nanofilter array is defined as $U^* = \widetilde{V}/(E_{\mathrm{av}} U_{\max})$, where $U_{\max}$ is the maximum sieving free mobility. Experimentally, the maximum sieving free mobility across the nanofilter array is obtained by extrapolation of the mobility curve to a zero length [14]. Size selectivity of the nanofilter device is characterized by the derivative of normalized mobility with respect to the DNA size, $\mathrm{d}U^*/\mathrm{d}N$ ($N$ is the size of DNA in bp). As shown in Fig. 5, the normalized mobility is dependent on both the electric fields and the DNA sizes. Low field strength leads to a steeper mobility slope, corresponding to a better size selectivity. However, reducing the electric field lengthens separation time, which will increase the dispersion and compromise the resolution of the separation. A tradeoff between the size selectivity, separation time, and peak dispersion is required to obtain optimized separation results.

### 3.4 Band dispersion

As shown in Fig. 6, the dispersion data obtained from the simulation are generally comparable in magnitudes to the experimental data. However, the model-predicted dispersion decreases as the DNA size or electric field strength increase, while the experimental data show an almost length- and field-independent dispersion behavior. These differences are mainly due to the simplicity of our simulation model.

The band broadening in this simulation model is caused by several mechanisms. The diffusive dispersion is induced by the random Brownian motion of the DNA molecules. The convective dispersion is due to the exponential decaying of the concentration with time as DNA molecules are traveling from one deep well to the next one (crossing the energy barrier in the shallow slits). In addition, there is another dispersion arising from the field nonuniformity (which provides different field lines for the molecules to take) in the deep well of the device. Our method models all these dispersion mechanisms appropriately. Among the three dispersion mechanisms discussed above, diffusive dispersion would be more severe for shorter DNA molecules, while the convective dispersion would be independent of the DNA length.

Other factors that are not considered in this article might include the stochastic dye attachment, the flexibility of DNA molecules, and Joule heating *etc.* Nonuniform dye labeling will definitely contribute to the dispersion (width of peak)

 

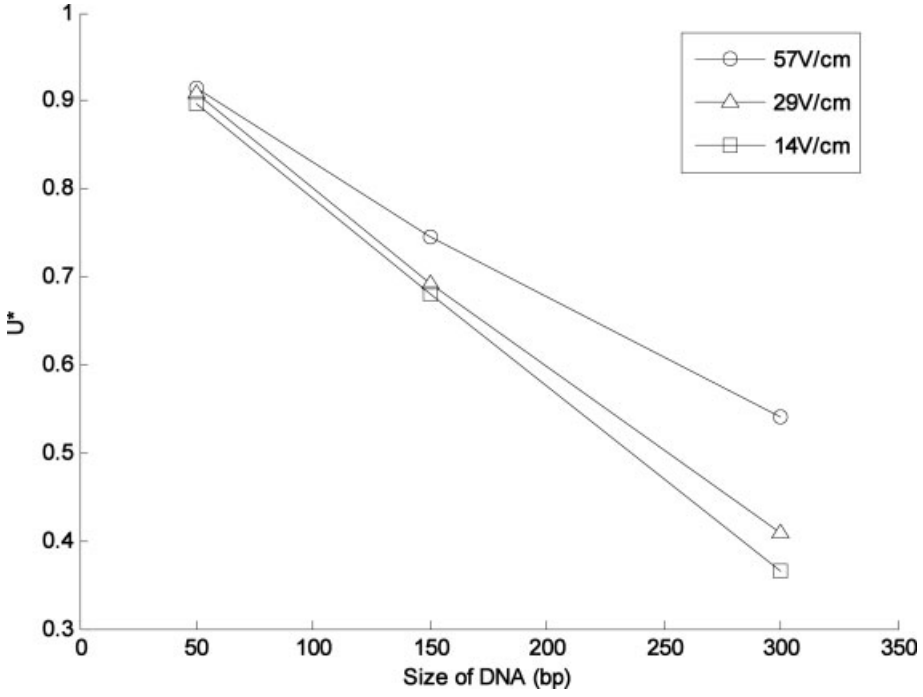


**Figure 5.** Dependence of relative mobility on DNA sizes under different electric field strengths calculated from simulation data with consideration of EOF. Lower electric field leads to a higher mobility difference for DNA sizes, or a higher selectivity.

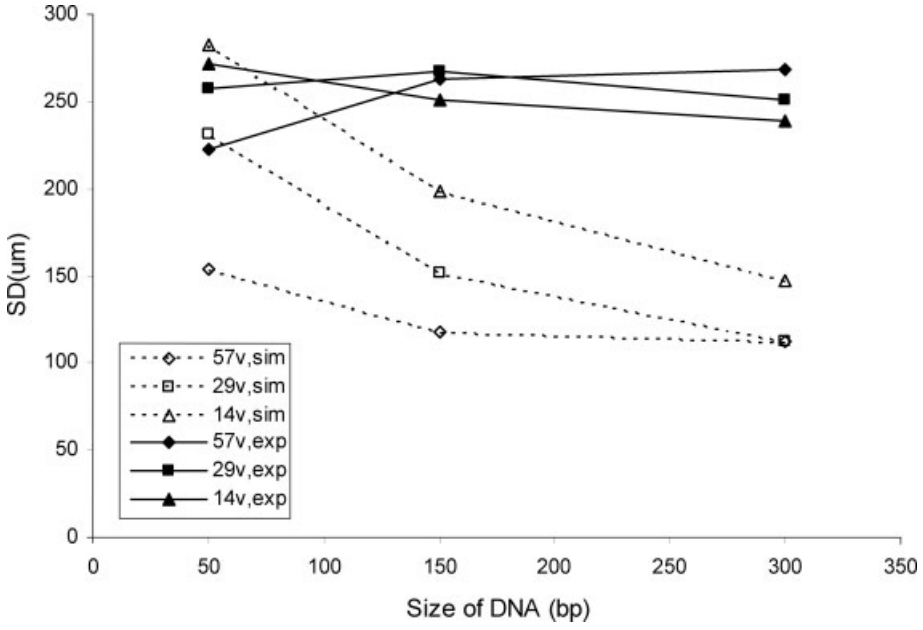


**Figure 6.** Experimental and simulation dispersions under different electric field strengths against DNA sizes. Compared with experimental data that are generally size and field independent, variances in simulation are dependent on both factors. The deviation between the experimental and simulation data is due to the simplicity of this model, in which only the diffusive dispersion and convective dispersion are considered. Other unconsidered factors that might contribute to dispersion may include flexibility of molecules, stochastic nature of dye attachment, *etc.*

because it causes the DNA molecules in the experiment to have slightly different free-solution electrophoretic mobility. Any modification of the electrophoretic mobility may cause significant alteration in the effective electrophoretic mobility in the presence of EOF. In addition, flexibility of the DNA molecules is certainly a factor that contributes to the mismatch between the experimental results and the simulation data. We do observe that the fitting is getting worse as the length of the chain increases, where the flexibility of the DNA increases. However, we do not believe that Joule heating is a factor in our experiments, simply because the nanochannels in the device are too thin (less than 500 nm, even in "deep" region). Therefore, the amount of current going through the system is tiny compared with other standard microfluidic systems. Any temperature shift in this system caused by Joule heating would be negligible [12, 14].

One should note that the selectivity of the nanofilter sieving systems is more straightforward to simulate, com-

 

pared with dispersion behavior. In most of the previous modeling of nanofilters and entropic trapping device [15–17], such as Brownian dynamics and dissipated participle dynamics, the selectivity is obtained by simulating the dynamics of a single DNA molecule through one nanofilter, while the absolute value of the electrophoretic mobility is usually one of the fitting parameters. Under such formulation, the physics that are neglected in the model are accounted for by the modifications in the (free solution) electrophoretic mobility. However, such a method does not work for calculation of dispersion. For these reasons, most of previous modeling studies focus mainly on the selectivity, not the dispersion. Our simulation model is developed to predict the dispersion, as well as the mobility, by solution of the continuum transport equation for a collection of molecules in a nonsteady-state condition. The magnitude of EOF is the only adjustable parameter that is used to fit the selectivity. Although dispersions in some cases are underestimated due to omission of some factors mentioned above, they are largely comparable in size. Based on the correctly predicted mobility and approximately estimated dispersion, a practical evaluation of the quality of a nanofilter array is still achievable.

The deviations between the simulation data and the experimental ones may also be due, in part, to the nonideal shape of the nanochannel devices. Our simulation is based on the ideal, square-shaped device structure, while the actual nanofilter devices have rather sloped sidewalls between nanochannels and deep wells [12]. In fact, micro/nanofluidic channel sidewalls are rarely ideal as shown in Fig. 1, which could have a significant impact on the separation of the molecules in the system, leading to modified sieving/dispersion characteristics. We are currently implementing this strategy to a device with sloped and nonideal deep well structures, in order to study and optimize the device structures.

## 4 Concluding remarks

This article proposed a simulation model based on anisotropic transport theory for simulating electrophoretic traveling of the rod-like DNA molecules over repeated regular nanofilter arrays. Unlike computationally expensive, stochastic methods such as Brownian dynamics, this method focuses on the behavior of a group of DNA molecules rather than a single one. It is therefore capable of investigating large time and length scale macroscopic phenomena. It also provides the estimation of peak dispersion, which is often computationally too expensive for stochastic modeling techniques. It is shown that the orientational entropy barrier in shallow slits plays a major role in the electrophoretic partitioning of the rod-like DNA molecules of different sizes across nanofilter arrays. In addition, the steric constraint in the shallow region increases the mobility of longer rod-like DNAs. This modification affects the separation results significantly if the mobility of EOF is comparable with the DNA's free-solution electrophoretic mobility. It helps to explain the complex experimental data of short DNA electrophoresis over flat nanochannels observed by Pennathur *et al.* [47] and Cross *et al.* [48]. More importantly, the realization that the rotational diffusion affects the partition of anisotropic particles (implemented through the mobility corresponding to the entropic force) has significant consequences in our understanding of many processes involving transport of anisotropic particles in nanochannels. These findings are critically important in design and optimization of nanofiltration devices for the separation of rod-like electrolytes and charged particles of other geometrical shapes.

*This work was funded by Singapore-MIT Alliance (SMA)-II, Computational Engineering (CE) programme. The authors express their thanks to Jianping Fu (MIT) for many helpful discussions. Also, thanks for Nicolas Hadjiconstantinou (MIT) for reading the paper and making valuable comments. Z. R. Li wishes to express his gratitude to former NUS Professor Nikolai K. Kocherginsky for his helpful advice and continuous encouragements.*

*The authors have declared no conflict of interest.*

## 5 References

[1] Viovy, J. L., *Rev. Mod. Phys.* 2000, *72*, 813–872.

[2] Ogston, A. G., *Trans. Faraday Soc.* 1958, *54*, 1754–1757.

[3] Rodbard, D., Chrambach, A., *Proc. Natl. Acad. Sci. USA* 1970, *65*, 970–977.

[4] Morris, C. J. O. R., *Protides Biol. Fluids* 1966, *14*, 543–551.

[5] Locke, B. R., Trinh, S. H., *Electrophoresis* 1999, *20*, 3331–3334.

[6] Allison, S. A., Li, Z., Reed, D., Stellwagen, N. C., *Electrophoresis* 2002, *23*, 2678–2689.

[7] Yuan, C., Rhoades, E., Heuer, D. M., Saha, S. X. *et al.*, *Anal. Chem.* 2006, *78*, 6179–6186.

[8] Muthukumar, M., Baumgartner, A., *Macromolecules* 1989, *22*, 1937–1941.

[9] Muthukumar, M., *Annu. Rev. Biophys. Biomol. Struct.* 2007, *36*, 435–450.

[10] Han, J., Turner, S. W., Craighead, H. G., *Phys. Rev. Lett.* 1999, *83*, 1688–1691.

[11] Han, J., Craighead, H. G., *Science* 2000, *288*, 1026–1029.

[12] Fu, J., Yoo, J., Han, J, *Phys. Rev. Lett.* 2006, *97*, 018103.

[13] Fu, J., Schoch, R. B., Stevens, A. L., Tannenbaum, S. R., Han, J., *Nat. Nanotech.* 2007, *2*, 121–128.

[14] Fu, J., Mao, P., Han, J., *Appl. Phys. Lett.* 2005, *87*, 263902.

[15] Fan, X. J., Phan-Thien, N., Chen, S., Wu, X. H., Ng, T. Y., *Phys. Fluids* 2006, *18*, 063102.

[16] Duong-Hong, D., Wang, J.-S., Liu, G. R., Chen, Y. Z. *et al.*, *Microfluid. Nanofluid.* 2007, *3*, DOI 10.1007/s10404-007-0170-7.

 

[17] Laachi, N., Declet, C., Matson, C., Dorfman, K. D., *Phys. Rev. Lett.* 2007, *98*, 098106.

[18] Kocherg-insky, N., Zhang, Y. K., *J. Phys. Chem. B* 2003, *107*, 7830–7837.

[19] Brenner, H., *J. Colloid Interface Sci.* 1979, *71*, 189–208.

[20] Han, Y., Alsayed, A. M., Nobili, M., Zhang, J. *et al.*, *Science* 2006, *314*, 626–630.

[21] Berg, H. C., *Random Walks in Biology*, Princeton University Press, Princeton, New Jersey, USA 1983.

[22] Mercier, J.-F., Slater, G. W., *Electrophoresis* 2006, *27*, 1453–1461.

[23] Stellwagen, E., Lu, Y. J., Stellwagen, N. C., *Biochemistry* 2003, *42*, 11745–11750.

[24] Stellwagen, E., Stellwagen, N. C., *Electrophoresis* 2002, *23*, 2794–2803.

[25] Allison, S. A., Mazur, S., *Biopolymers* 1998, *46*, 359–373.

[26] Eimer, W., Pecora, R., *J. Chem. Phys.* 1991, *94*, 2324–2329.

[27] Tirado, M. M., Martinez, C. L., Garcia de la Torre, J., *J. Chem. Phys.* 1984, *81*, 2047–2052.

[28] Tinland, B., Meistermann, L., Weill, G., *Phys. Rev. E* 2000, *61*, 6993–6998.

[29] Arvanitidou, E., Hoagland, D., *Phys. Rev. Lett.* 1991, *67*, 1464–1466.

[30] Stellwagen, N. C., Gelfi, C., Righetti, P. G., *Biopolymers* 1997, *42*, 687–703.

[31] Happel, J., Brenner, H., *Low Reynolds Number Hydrodynamics*, Kluwer Academic Publishers, Dordrecht, The Netherlands 1991.

[32] Ohshima, H., *J. Colloid Interface Sci.* 1996, *180*, 299–301.

[33] Levine, A. J., Liverpool, T. B., MacKintosh, F. C., *Phys. Rev. E* 2004, *69*, 021503.

[34] Nkodo, A. E., Garnier, J. M., Tinland, B., Ren, H. *et al.*, *Electrophoresis* 2001, *22*, 2424–2432.

[35] Giddings, J. C., Kucera, E., Russell, C. P., Myers, M. N., *J. Phys. Chem.* 1968, *72*, 4397–4408.

[36] Kratky, O., Porod, G., *Recl. Trav. Chim. Pays-Bas* 1949, *68*, 1106–1123.

[37] Marko, J. F., Siggia, E. D., *Macromolecules* 1995, *28*, 8759–8770.

[38] Kihm, K. D., Banerjee, A., Choi, C. K., Takagi, T., *Exp. Fluids* 2004, *37*, 811–824.

[39] Pennathur, S., Santiago, J. G., *Anal. Chem.* 2005, *77*, 6772–6781.

[40] Pennathur, S., Santiago, J. G., *Anal. Chem.* 2005, *77*, 6782–6789.

[41] Cummings, E. B., Griffiths, S. K., Nilson, R. H., Paul, P. H., *Anal. Chem.* 2000, *72*, 2526–2532.

[42] Lucy, L. B., *Astron. J.* 1977, *83*, 1013–1024.

[43] Liu, G. R., Liu, M. B., *Smoothed Particle Hydrodynamics - A Mesh-Free Particle Method*, World Scientific, Singapore 2003.

[44] Monaghan, J. J., *Rep. Progr. Phys.* 2005, *68*, 1703–1759.

[45] Kum, O., Hoover, W. G., Posch, H. A., *Phys. Rev. E* 1995, *52*, 4899–4908.

[46] Giddings, J. C., *Unified Separation Science*, John Wiley & Sons, New York 1991.

[47] Pennathur, S., Baldessari, F., Santiago, J. G., Kattah, M. *et al.*, *Anal. Chem.*, 2007, *79*, 8316–8322.

[48] Cross, J. D., Strychalski, E. A., Craighead, H. G., *J. Appl. Phys.* 2007, *102*, 024701.

 